

Determination of activation energy of ion-implanted deuterium release from W-Y_2O_3

Xue-Feng Wang(王雪峰), Ji-Liang Wu(吴吉良), Qiang Li(李强), Rui-Zhu Yang(杨蕊竹), Zhan-Lei Wang(王占雷), Chang-An Chen(陈长安), Chun-Rong Feng(冯春蓉), Yong-Chu Rao(饶咏初), Xiao-Hong Chen(谌晓洪), Xiao-Qiu Ye(叶小球)

Citation: Chin. Phys. B . 2020, 29(6): 065205 . **doi:** 10.1088/1674-1056/ab8204
Journal homepage: http://cpb.iphy.ac.cn; http://iopscience.iop.org/cpb

What follows is a list of articles you may be interested in

Developing cold-resistant high-adhesive electronic substrate for WIMPs detectors at CDEX

Yuanyuan Liu(刘圆圆), Jianping Cheng(程建平), Pan Pang(庞盼), Bin Liao(廖斌), Bin Wu(吴彬), Minju Ying(英敏菊), Fengshou Zhang(张丰收), Lin Chen(陈琳), Shasha Lv(吕沙沙), Yandong Liu(刘言东), Tianxi Sun(孙天希)

Chin. Phys. B . 2020, 29(4): 045203 . **doi:** 10.1088/1674-1056/ab718a

Composition effect on elastic properties of model NiCo-based superalloys

Weijie Li(李伟节), Chongyu Wang(王崇愚)

Chin. Phys. B . 2020, 29(2): 026102 . **doi:** 10.1088/1674-1056/ab6204

First-principles studies on carbon diffusion in tungsten

Chi Song(宋驰), Xiang-Shan Kong(孔祥山), C S Liu(刘长松)

Chin. Phys. B . 2019, 28(11): 116106 . **doi:** 10.1088/1674-1056/ab4bb9

Stability and mechanical properties of various Hf-H phases:A density-functional theory study

Wei Xiao(肖伟), Lu Sun(孙璐), Shu-Hui Huang(黄树晖), Jian-Wei Wang(王建伟), Lei Cheng(程磊), Li-Gen Wang(王立根)

Chin. Phys. B . 2017, 26(10): 106103 . **doi:** 10.1088/1674-1056/26/10/106103

The effects of substrate temperature on ZnO-based resistive random access memory devices

Zhao Jian-Wei, Liu Feng-Juan, Huang Hai-Qin, Hu Zuo-Fu, Zhang Xi-Qing

Chin. Phys. B . 2012, 21(6): 065201 . **doi:** 10.1088/1674-1056/21/6/065201

Determination of activation energy of ion-implanted deuterium release from W–Y_2O_3*

Xue-Feng Wang(王雪峰)[1,2], Ji-Liang Wu(吴吉良)[2], Qiang Li(李强)[2], Rui-Zhu Yang(杨蕊竹)[2], Zhan-Lei Wang(王占雷)[2], Chang-An Chen(陈长安)[2], Chun-Rong Feng(冯春蓉)[1,2], Yong-Chu Rao(饶咏初)[2], Xiao-Hong Chen(谌晓洪)[1,†], and Xiao-Qiu Ye(叶小球)[2,‡]

[1] *School of Sciences and Research Center for Advanced Computation, Xihua University, Chengdu* 610039, *China*
[2] *Science and Technology on Surface Physics and Chemistry Laboratory, Mianyang* 621907, *China*

(Received 6 January 2020; revised manuscript received 5 March 2020; accepted manuscript online 23 March 2020)

The retention and release of deuterium in W–2%Y_2O_3 composite materials and commercially pure tungsten after they have been implanted by deuterium plasma (flux $\sim 3.71\times10^{21}$ D/m^2·s, energy $\sim$ 25 eV, and fluence up to 1.3×10^{26} D/m^2) are studied. The results show that the total amount of deuterium released from W–2%Y_2O_3 is 5.23×10^{20} D/m^2(2.5 K/min), about 2.5 times higher than that from the pure tungsten. Thermal desorption spectra (TDS) at different heating rates (2.5 K/min–20 K/min) reveal that both W and W–2%Y_2O_3 have two main deuterium trapped sites. For the low temperature trap, the deuterium desorption activation energy is 0.85 eV (grain boundary) in W, while for high temperature trap, the desorption activation energy is 1.57 eV (vacancy) in W and 1.73 eV (vacancy) in W–2%Y_2O_3.

Keywords: metals and alloys, plasma-based ion implantation, thermal desorption, diffusion in solid

PACS: 61.82.Bg, 52.77.Dq, 68.43.Vx, 66.30.–h **DOI:** 10.1088/1674-1056/ab8204

1. Introduction

Tungsten has been considered as one of the candidate PFMs for ITER because of its favorable physical and chemical properties, such as high thermal conductivity, high melting point, high-temperature mechanics performance, low physical and chemical sputtering yields, and no chemical reaction with hydrogen.[1–7] However, the brittleness of W material leads PFM to likely undergo crack failure when the transient event occurs.[8]

W–Y_2O_3 alloys can effectively impede the recovery and recrystallization at high temperature, and have low ductile–brittle transition temperature (DBTT) compared with pure tungsten.[12,13] Tan *et al.*[14] prepared and studied the mechanical properties and microstructure changes of W–Y_2O_3 alloy under helium irradiation, the results showed that W–Y_2O_3 have the trend of lattice distortion, polycrystal and phase transformation. Yao *et al.*[15] studied the surface damage of W–Y_2O_3 irradiated by helium. The results showed that the grain orientation of W–Y_2O_3 irradiated by helium ion changes obviously and helium bubbles gather near the surface phase interface. The surface damage and hydrogen isotope retention of W–Y_2O_3 exposed to deuterium plasma have been investigated, the experimental results of Tan[16] showed that the retention of deuterium is related to the texture and laminated microstructure of the irradiated surface of the sample. The results of Zhao[17] showed that the blisters and deuterium retention of W–Y_2O_3 are strongly dependent on the injection temperature. However, the desorption activation energy of deuterium in W–Y_2O_3 is rarely reported.

In this work, based on the research of Yao *et al.*, the deuterium desorption activation energy in W–2%Y_2O_3 composite material and commercial pure tungsten after being exposed to deuterium plasma are experimentally determined by thermal desorption spectroscopy. The differences in deuterium retention and release between W–2%Y_2O_3 and W are discussed.

2. Experimental details

2.1. Sample preparation

W–2%vol Y_2O_3 was supplied by Hefei University of Technology, which was prepared by using the wet chemistry combined with plasma sintering,[18,19] and the pure-W was obtained from ATTL www.tlwm.cn) with a purity of 99.95 wt%. All samples were hot rolled with the rolling ratio of 50%, and then were fabricated into square pieces with 10 mm $\times$10 mm$\times$1 mm from the same manufacturing batch. The surfaces were mechanically polished to a mirror-like finish then ultrasonically cleaned in acetone and ethanol. Finally, all samples were annealed at 1273 K under vacuum better than 5×10^{-5} Pa for 1 h to relieve residual stresses generated in the grinding and polishing process.

*Project supported by the National Magnetic Confinement Fusion Energy Research Project, Ministry of Science and Technology of China (Grant No. 2015GB109002), the Innovation Fund of Postgraduate, Xihua University, China (Grant No. ycjj2018017), and the National Natural Science Foundation of China (Grant No. 21401173).

†Corresponding author. E-mail: shengxiaohongb@163.com
‡Corresponding author. E-mail: xiaoqiugood@sina.com

© 2020 Chinese Physical Society and IOP Publishing Ltd

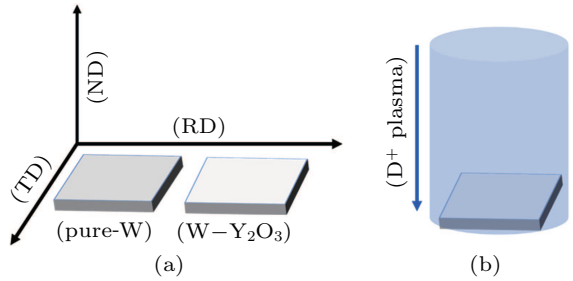


Fig. 1. (a) RD, TD, and ND represent rolling direction, transverse direction, and normal direction, respectively, and (b) schematic diagram of plasma implantation direction.

2.2. Methods

Deuterium ion irradiation was conducted by using comprehensive ECR plasma for tritium (CEPT) generating device in the Science and Technology on Surface Physics and Chemistry Laboratory.

The ion implantation direction is perpendicular to the rolling direction (RD)–transverse direction (TD) surface of the material (as shown in Fig. 1).

The detailed conditions of the deuterium ion irradiation are listed in Table 1. The pressure of deuterium (purity: 99.999%) was fixed at 0.7 Pa in the irradiation chamber during its operation. The energy of the deuterium ions and the flux were obtained by the langmuir probe. During deuterium ion irradiation, the samples were 375 K according to the measurements obtained by S-type thermocouple contacting the back of the samples.

Table 1. Detailed experiment conditions for pure-W and W–Y_2O_3.

Sample	Materials	Ion species	Ion energy/eV	Ion flux/(ions/m^2·s)	Ion fluence/(D/m^2)	Temperature/K
1–4	pure-W	D	25	3.71×10^{21}	1.3×10^{26}	375
5–8	W–Y_2O_3	D	25	3.71×10^{21}	1.3×10^{26}	375

After the samples are irradiated by deuterium ions, the deuterium retention and desorption activation energy in the sample were obtained by using thermal desorption spectroscopy device[20] in the Science and Technology on Surface Physics and Chemistry Laboratory. The pipe which the ions passed through was baked for 72 h to remove residual gas in the material prior to the TDS experiment. The samples were heated by linearly increasing the temperature up to 1273 K at different heating rates (Table 2) in the quartz tube under vacuum better than 10^{-6} Pa. In addition, in order to quantitatively calculate the deuterium retention, D_2 ($m/z=4$) and HD ($m/z=3$) signal were tracked by quadrupole mass spectrometer (QMS), and the D_2/H_2 signal was calibrated by using two standard leaks after experiment. The HD signal was the average of the sum of D_2 and H_2 signals. The x-ray diffraction (XRD) and scanning electron macroscopy (SEM) were also used to characterize the non-irradiated and irradiated samples.

Table 2. Heating rate for pure-W and W–Y_2O_3 in TDS experiment.

Sample	1	2	3	4	5	6	7	8
Heating rate/(K/min)	2.5	5	10	20	2.5	5	10	20

3. Results and discussion

3.1. Sample characterization

Figures 2(a) and 2(b) show the orientation image maps of the W and W–Y_2O_3, characterized by the electron backscattered diffraction (EBSD). It can be seen from Fig. 2(c) that red color and blue color are dominant in Fig. 2(a), corresponding to (100) and (111) crystal plane, respectively; dominant in Fig. 2(b) are red color, blue color, and green color, corresponding to (100), (111), and (110) crystal planes. Figures 2(a) and 2(b) show that there are (100) and (111) textures on the RD–D surface of W and (100), (111), and (110) textures on the RD–TD surface of W–Y_2O_3.

The surface morphology of W and W–Y_2O_3 irradiated by deuterium ions confirm this point (Figs. 2(d)–2(e))). After irradiation, the surface of W is covered with a large number of small blisters (∼ 100 nm in size, see Fig. 5(d)), The blisters on the surface of W–Y_2O_3 are much larger than those on the surface of W (∼ 2 μm in size), accompanied by the bulges of the substrate (Fig. 2(e)).

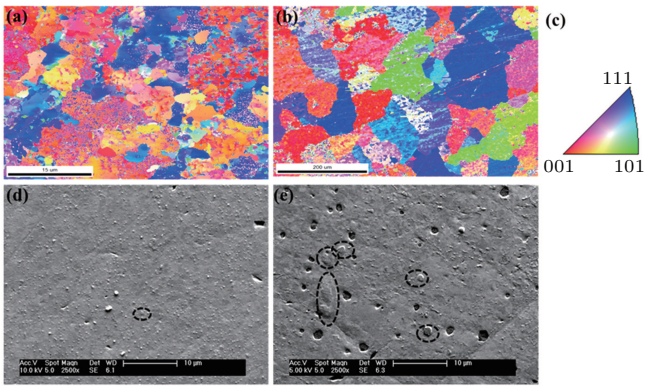


Fig. 2. EBSD images of (a) W and (b) W–Y_2O_3 before being irradiated by deuterium ions, (c) legend for panels (a) and (b), SEM images of (d) W and (e) W–Y_2O_3 after being irradiated by deuterium ions.

Pan *et al.*[21] showed that the potential barrier for H ions to diffuse into the surface is larger than that into the bulk phase, and H ions preferentially accumulate on the W (111) surface compared with on the bulk phase, and W (110) is the resistance surface for the formation of H blisters. Figures 2(a) and 2(b) show that there are a large number of other oriented crystal planes in the red region of the RD–TD plane of W, which leads

the red region to fragment, while the color boundary of the RD–TD plane of W–Y_2O_3 is obvious, the other orientations of the RD–TD plane are few, and the average grain boundary size is much larger than that of W. Figures 2(d) and 2(e) show that the deuterium blisters with small size ($\sim$ 100 nm) are produced on the surface of W during irradiation, and deuterium blisters with larger size ($\sim$ 2 μm) appear in some areas of W–Y_2O_3. This is consistent with Pan's conclusion.

Figure 3 shows the XRD spectra of the main characteristic peaks of W and W–Y_2O_3 before and after being irradiated by the deuterium ions. In Fig. 3(a) the normal XRD peak of W in the original state, as a reference standard XRD spectrum, reflects the isotropic characteristics. As shown in Fig. 3(b), the peak position (2θ) of the irradiated W has a slight leftward shift of 0.08° compared with the peak of the non-irradiated sample, while the peak position of W–Y_2O_3 shifted 0.2° to the left after being irradiated by the deuterium ions. Table 3 shows the the lattice constant of W is increased by 0.009 Å while that of W–Y_2O_3 by 0.014 Å.

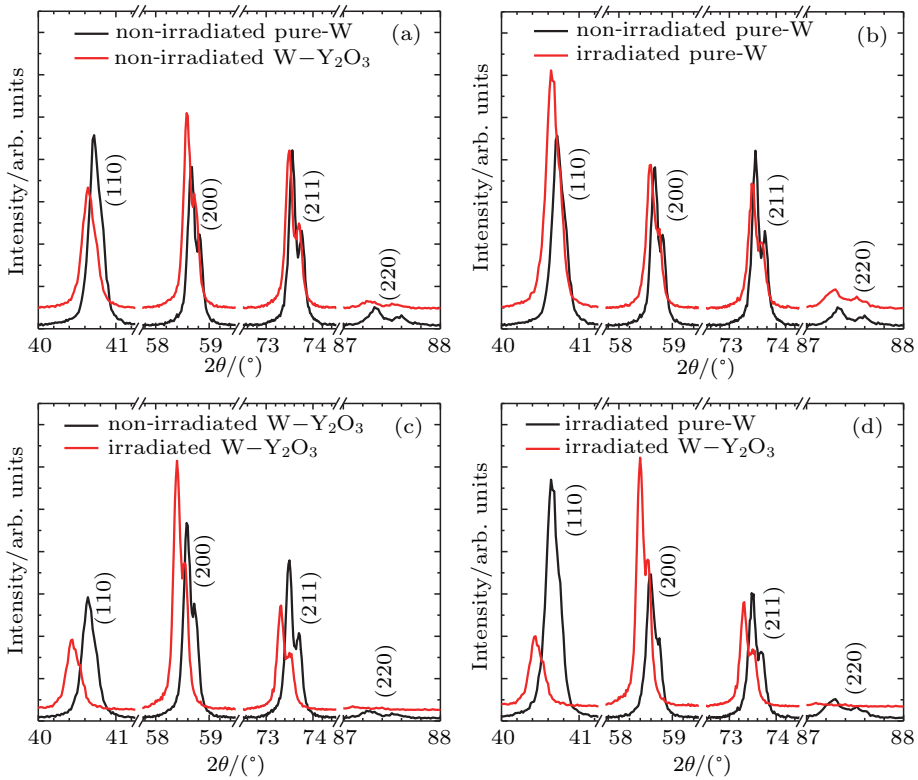


Fig. 3. XRD patterns of pure-W and W–Y_2O_3 before and after being irradiated, for (a) non-irradiated pure-W and W–Y_2O_3 samples; (b) pure-W before and after being irradiated; (c) W–Y_2O_3 before and after being irradiated; (d) irradiated pure-W and W–Y_2O_3 samples.

Table 3. Lattice constants of pure-W and W–Y_2O_3 before and after being irradiated.

	Pure-W/Å	W–Y_2O_3/Å
Non-irradiated	3.137	3.143
Irradiated	3.146	3.157

3.2. Deuterium release and retention

Figures 4(a) and 4(b) show the D_2 TDS spectra of W and W–Y_2O_3. As expected, when the heating rate increases, the main desorption peaks of deuterium in W and W–Y_2O_3 extend to the high temperature section and the peak shape intensity is enhanced due to non-diffusion deuterium.[20]

The TDS spectra show the macroscopic characteristics of deuterium released from the whole sample, which is formed by coupling the different deuterium trap release peaks in the sample. The TDS spectra of W–Y_2O_3 and W have obvious shoulder peaks near 600 K, indicating that there is a corresponding low temperature deuterium trap in the sample. The whole release peak can be divided into the coupling of the release peaks of the low temperature traps (LTTs) and the high temperature traps (HTTs) (Figs. 4(a) and 4(b)).

The TDS peak of W and W–Y_2O_3 are in accordance with Gauss distribution. According to the results of the reaction kinetics in differential thermal analysis of Kissinger,[22] the desorption activation energy can be calculated from the TDS spectra with different heating rates by the following formula:

$$\frac{\partial \ln(\beta/T_p^2)}{\partial(1/T_p)} = -\frac{E_a}{R}, \tag{1}$$

where β is the heating rate, T_p is the temperature of the peak of the TDS spectrum, E_a is the desorption activation energy of sample, and R is the universal gas constant.

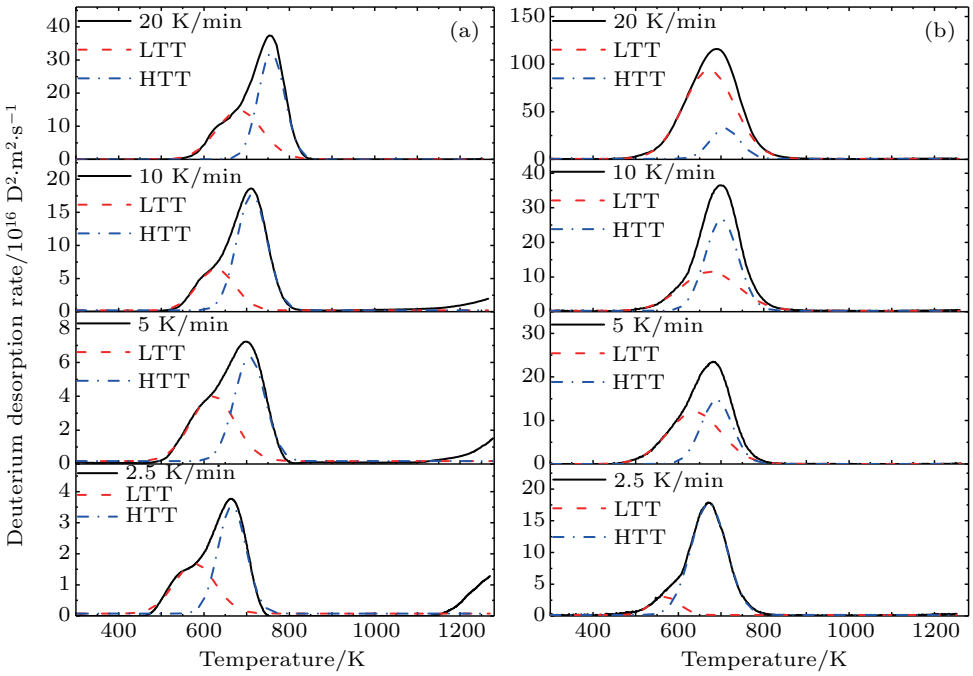


Fig. 4. TDS spectra of (a) W and (b) W–Y_2O_3 at different heating rates.

Since β and T_p are known, the evoluation of desorption activation energy E_a of deuterium ion from a trapping site can be calculated from the slope of the $\ln(\beta/T_p^2)$ *versus* $(1/T_p)$ plot. The results are shown in Fig. 5. The fitting results have good linear relationship and satisfy the Arrehenius relationship. The results show that the E_a value of W–Y_2O_3 is 0.39 eV for LTT ($\sim$ 600 K) and 1.73 eV for HTT ($\sim$ 700 K), while the E_a value of pure W is 0.86 eV for LTT ($\sim$ 600 K) and 1.57 eV for HTT ($\sim$ 700 K) as shown in Fig. 5.

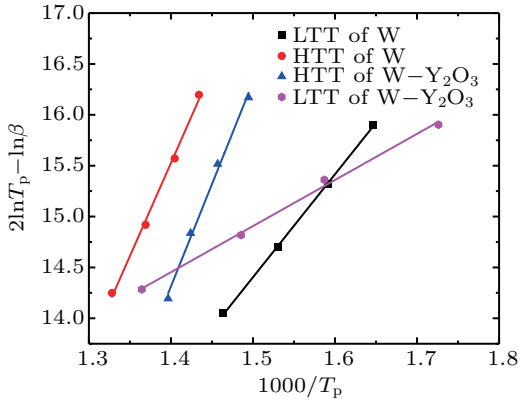


Fig. 5. Plots of desorption activation energies of LTT and HTT of W and W–Y_2O_3 by least squares fitting, where line is least square fitting.

Table 4. Desorption activation energy of deuterium in W.

	Desorption activation energy/eV
Migration barrier	0.35–0.38,[23] 0.39[24]
Dislocation (D) or Grain boundary (D)	0.85[25]
Vacancy (D)	1.07–1.55,[24–27] 1.79[28]
Vacancy cluster (D)	1.80–2.34[24,26,29]
Vacancy cluster (D_2)	1.45,[29] 1.4[24]

According to the experimental and modeling results (see Table 4), the values E_a of 0.39 eV and 0.86 eV are close to those explained as the migration of deuterium atoms between LTTs such as interstitials, dislocations, and grain/phase boundaries. The smaller value of E_a for LTT in W–Y_2O_3 is in acoordance with the fact that there are more phase boundaries in W–Y_2O_3 due to the doping effects. Obviously, the values of E_a of 1.57 eV and 1.73 eV for HTT can be attributed to deuterium atoms in vacancies. Interestingly, the value of E_a for HTT in W–Y_2O_3 is higher than that in pure W. Considering that the blisters on the surface of W–Y_2O_3 are larger than those of pure W, we think that there may be vacancy clusters in W–Y_2O_3.

It is worth mentioning that some deuterium atoms even are desorbed from pure W at very high temperature (1200 K) (Fig. 4), while W–Y_2O_3 has no such behavior. The origin of such differences is not fully clear. It may be due to the fact that deuterium atoms gather on the subsurface of W–Y_2O_3, giving rise to blisters and leading to more defects. The capture of deuterium atoms by these defects prevents the deuterium atoms from diffuing to deeper depths. Qiu *et al.*[30] also found that the trapping of positions may prevent hydrogen isotope from diffusing and also from accumulating their concentration on the shallow substrate. However, for pure W, part of the deuterium atoms are captured in the sublayer; more deuterium atoms will diffuse into the bulk. Figure 6 shows that the deuterium content of W–Y_2O_3 is much higher than that of W in a depth range of 0 nm–2000 nm, which is in good agreement with Qiu's conclusion.

The results of Zhou *et al.*[31] showed that without consid-

ering the effect of temperature, most of the H atoms occupy the interstitial positions in the bulk phase, while only some H atoms occupy the defects related to the vacancies. Therefore, most of the deuterium atoms in W–Y_2O_3 are mainly concentrated at the interstitial positions near the surface layer, while most of the deuterium atoms in W are distributed at the interstitial positions in the whole bulk phase, which may be the reason why the deuterium release peak at the interstitial position in W–Y_2O_3 is observed in the TDS spectrum, but the deuterium release peak at the interstitial position in W cannot be observed obviously.

Figure 7 shows the deuterium retention of W and W–Y_2O_3, when considering the contribution of LTT and HTT respectively. In the W–Y_2O_3, the contribution of deuterium from LTT to the total amount zigzags upward with the increase of the heating rate, and finally exceeds the contribution of HTT to the total amount (Fig. 7(b)). However, for W (Fig. 7(c)), with the increase of heating rate, the deuterium release in HTT is always higher than that in LTT.

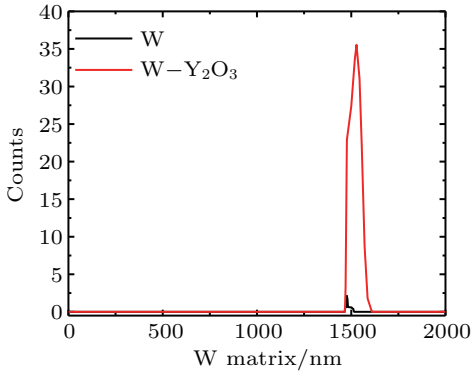


Fig. 6. NRA determined deuterium depth profile (topmost 2000 nm) for W and W–Y_2O_3 exposed to deuterium plasma.

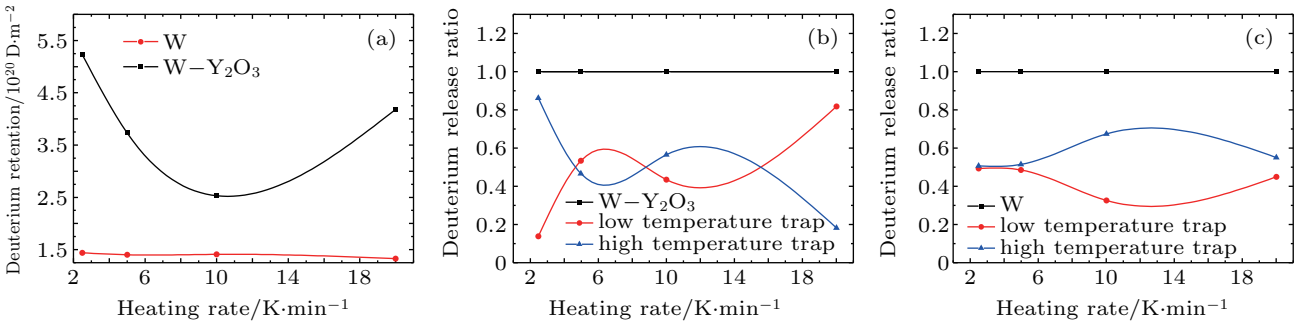


Fig. 7. (a) Deuterium retentions of W and W–Y_2O_3 with different heating rates; deuterium releases of LTT and HTT of (b) W–Y_2O_3; (c) W.

4. Conclusions

The deuterium retention and release in Y_2O_3 doped by tungsten, exposed to high-flux low-energy plasma, is studied. The total number of deuterium atoms released from W–Y_2O_3 is 5.23×10^{20} D/m^2 (2.5 K/min), about 2.5 times higher than that from pure tungsten. The W–Y_2O_3 has two main deuterium trapped sites. For low temperature traps, the desorption activation energy is 0.39 eV while for high temperature traps (vacancy), the desorption activation energy is 1.73 eV. Both low temperature traps and high temperature traps make important contributions to trapping D.

Acknowledgment

We thank the School of Materials of Hefei University of Technology for providing the samples, the School of Physics of Peking University for assistance, and the State Key Laboratory of Nuclear Physics and Technology for the NRA experiment. We also thank Dr. Jiang C L and Dr. Tan X for their helpful comments on the manuscript.

References

[1] Tokunaga K, Baldwin M J , Doerner R P, Noda N, Kubota Y, Yoshida N, Sogabe T, Kato T and Schedler B 2005 *J. Nucl. Mater.* **337–339** 887
[2] Davis J W, Barabash V, Makhankov A Plochl L and Slattery K T 1998 *J. Nucl. Mater.* **256–263** 308
[3] Alimov V K, Hatano Y, Tyburskapuschel B, Sugiyama K, Takagi I, Furuta Y, Dorner J, Fuseder M, Isobe K, Yamanishi T and Matsuyama M 2013 *J. Nucl. Mater.* **441** 280
[4] Ou J, Xiang N, Men Z Z, Zhang L, Xu J C and Gao W 2019 *Chin. Phys. B* **28** 125201
[5] Zhang H, Wen S L, Pan M, Huang Z, Zhao Y, Liu Y and Chen J M 2016 *Chin. Phys. B* **25** 056102
[6] Wang J, Zhang H and Cheng X L 2013 *Chin. Phys. B* **22** 085201
[7] Sang C F, Dai S Y, Sun J Z, Bonnin X, Xu Q, Ding F and Wang D Z 2014 *Chin. Phys. B* **23** 115201
[8] Wirtz M, Linke J, Pintsuk G, Singheiser L and Zlobinski M 2013 *J. Nucl. Mater.* **438** S833
[9] Yar M, Wahlberg S, Bergqvist H, H Salem G, Johnsson M and Muhammed M 2011 *J. Nucl. Mater.* **412** 227
[10] Veleva L, Schaeublin R, Battabyal M, Plociski T and Baluc N 2015 *Int. J. Refract. Met. Hard Mater.* **50** 210
[11] Kim Y, Lee K H, Kim E, Cheong D and Hong S H 2009 *Int. J. Refract. Met. Hard Mater.* **27** 842
[12] Uytdenhouwen I, Decréton M, Hirai T, Linke J, Pintsuk G and Oost G V 2007 *J. Nucl. Mater.* **363–365** 1099
[13] Smid I, Akiba M, Vieider G and Plochl L 1998 *J. Nucl. Mater.* **258–263** 160
[14] Tan X, Luo L, Chen H, Zhu X, Zan X, Luo G, Chen J, Li P, Cheng J, Liu D and Wu Y 2015 *Sci. Rep.* **5** 12755
[15] Yao G, Luo L, Tan X Y, Zan X, Xu Q, Zhu X Y, Lu E, Cao X Z, Cheng J G and Wu Y C 2019 *Materialia* **6** 100268

[16] Tan Y, Lian Y, Feng F, Chen Z, Wang J, Liu X, Guo W, Cheng L and Lu G 2018 *J. Nucl. Mater.* **509** 145
[17] Zhao M, Jacob W, Manhard A, Gao L, Balden M, Von Toussaint U and Zhou Z 2017 *J. Nucl. Mater.* **487** 75
[18] Xu M Y, Luo L M, Lin J S, Xu Y, Zan X, Xu Q, Tokunaga K, Zhu X Y and Wu Y C 2018 *J. Alloys Compd.* **766** 784
[19] Wang Y C, Yao Z T, Cheng X W, Wu F Y and Wang F C 2007 *J. B. Inst. Thechnol.* **27** 824
[20] Wang Z, Chen C A, Song Y, Xiang X, Wang W, Liu L and Wang B 2018 *Fusion Eng.* **126** 139
[21] Pan G, Zhang Y, Li Y, Zhang C H, Zhao Z and Zeng Z 2017 *Int. J. Mod. Phys. C* **28** 1750090
[22] Kissinger H E 1957 *Anal. Chem.* **29** 1702
[23] Degtyarenko N N and Pisarev A A 2015 *Phys. Procedia* **71** 30
[24] Eleveld H 1996 *Hydrogen and helium in selected fusion reactor materials* (Ph.D. Dissertation) (Netherlands: Delft University of Technology) (in Netherlands)
[25] Ogorodnikova O V, Roth J and Mayer M 2003 *J. Nucl. Mater.* **313–316** 469
[26] Poon M, Haasz A A and Davis J W 2008 *J. Nucl. Mater.* **374** 390
[27] Heinola K and Ahlgren T 2010 *Phys. Rev. B* **81** 073409
[28] Johnson D F and Carter E A 2010 *J. Mater. Res.* **25** 315
[29] Ogorodnikova O V, Roth J and Mayer M 2008 *J. Appl. Phys.* **103** 034902
[30] Qiu M, Zhai L, Cui J, Fu B, Li M and Hou Q 2018 *Chin. Phys. B* **27** 073103
[31] Zhou H, Liu Y, Jin S, Zhang Y, Luo G N and Lu G H 2010 *Nucl. Fusion* **50** 115010